

Random-phase-approximation-based correlation energy functionals: Benchmark results for atoms

Hong Jiang^{a)} and Eberhard Engel

Center for Scientific Computing, J. W. Goethe-Universität Frankfurt, Max-von-Laue-Straße 1, D-60438 Frankfurt/Main, Germany

(Received 5 July 2007; accepted 17 September 2007; published online 14 November 2007)

The random phase approximation for the correlation energy functional of the density functional theory has recently attracted renewed interest. Formulated in terms of the Kohn-Sham orbitals and eigenvalues, it promises to resolve some of the fundamental limitations of the local density and generalized gradient approximations, as, for instance, their inability to account for dispersion forces. First results for atoms, however, indicate that the random phase approximation overestimates correlation effects as much as the orbital-dependent functional obtained by a second order perturbation expansion on the basis of the Kohn-Sham Hamiltonian. In this contribution, three simple extensions of the random phase approximation are examined; (a) its augmentation by a local density approximation for short-range correlation, (b) its combination with the second order exchange term, and (c) its combination with a partial resummation of the perturbation series including the second order exchange. It is found that the ground state and correlation energies as well as the ionization potentials resulting from the extensions (a) and (c) for closed subshell atoms are clearly superior to those obtained with the unmodified random phase approximation. Quite some effort is made to ensure highly converged data, so that the results may serve as benchmark data. The numerical techniques developed in this context, in particular, for the inherent frequency integration, should also be useful for applications of random phase approximation-type functionals to more complex systems. © 2007 American Institute of Physics. [DOI: 10.1063/1.2795707]

I. INTRODUCTION

Recent years have seen a revival of interest in the random phase approximation (RPA) and its extensions, both in the framework of Kohn-Sham density functional theory^{1–17} (KS-DFT) and within Green's function-based many-body theory for ground state properties.^{18–22} Within KS-DFT, the RPA for the energy and response function of the homogeneous electron gas played an important role in the development of the local-density approximation (LDA) as well as the generalized gradient approximation (GGA) for the exchange-correlation (XC) energy functional E_{xc} .^{23,24} Current interest in the RPA is stimulated by the concept of orbital-dependent (implicit) XC functionals, in which the XC energy is represented in terms of the KS orbitals and eigenenergies.^{25–29} Within this approach a RPA-type correlation energy functional is most easily formulated on the basis of the KS response function. Compared to LDA/GGA-type explicit XC functionals, implicit functionals have several attractive features: (1) The exchange can be treated exactly, leading to exchange energies and potentials which are free of self-interaction;³⁰ (2) the long-range dispersion interaction can be correctly described;^{1,17,31,32} (3) static correlation effects can be incorporated even within a spin-unpolarized formalism.¹²

A systematic formulation of orbital-dependent XC func-

tionals is possible within KS-based many-body theory, i.e., by using the KS Hamiltonian as noninteracting reference Hamiltonian in the framework of standard many-body theory (KS-MBT).^{27,33,34} In this approach the exact exchange of DFT emerges as a first order contribution to a straightforward perturbation expansion in powers of e^2 . All higher order terms constitute the DFT correlation energy. The lowest order correlation contribution resulting from perturbation theory $E_c^{(2)}$ has been extensively studied for atoms and small molecules.^{31,32,35–38} $E_c^{(2)}$ correctly accounts for the dispersion interaction^{31,32} and the corresponding correlation potential $v_c^{(2)}$ reproduces the shell-structure and asymptotic behavior of atomic correlation potentials.³⁸ On the other hand, the magnitude of the energies and potentials resulting from $E_c^{(2)}$ overestimates the corresponding exact data significantly. Moreover, $E_c^{(2)}$ is found to be variationally unstable for systems with a very small energy gap between the highest occupied and the lowest unoccupied molecular orbital^{37,38} (HOMO-LUMO gap) (as, for instance, the beryllium atom) and fails to describe chemical bonding in such elementary molecules as the nitrogen dimer.²⁷ The variational instability of $E_c^{(2)}$ can be resolved by resummation of suitable higher order contributions to infinite order (e.g., in the form of Feynman diagrams). The simplest functional of this type is obtained by resummation of selected ladder-type diagrams, i.e., the Epstein-Nesbet (EN) diagrams. The resulting functional is not only found to be variationally stable for all neutral and singly ionized atoms, but also gives more accurate correlation energies and potentials than $E_c^{(2)}$.³⁹ However,

^{a)}Current address: Fritz-Haber-Institut der Max-Planck-Gesellschaft, Faradayweg 4-6, D-14195 Berlin, Germany. Electronic mail: jiang@fhi-berlin.mpg.de

EN-type functionals still face fundamental problems in the case of degenerate or near-degenerate systems. A more suitable partial resummation scheme is needed to establish a universally applicable, implicit XC functional, where the RPA and its extensions being the prime candidates.

In standard many-body theory, the RPA is obtained by resummation of the so-called ring diagrams.⁴⁰ This concept can be directly transferred to the framework of KS-MBT.⁴¹ On the other hand, in the context of DFT, the RPA can also be derived from the adiabatic connection fluctuation-dissipation (ACFD) theorem.⁴² The ACFD formalism is, for instance, the conceptual starting point for the recent development of van-der-Waals DFT.¹ It has also been applied directly to various systems, including jellium surfaces and slabs,³ atoms,^{21,43} small molecules,^{9,10,15,22} and solids.^{11,17} All these calculations have demonstrated promising features of RPA-based functionals. On the other hand, the results for atoms,^{21,43} for which rigorous benchmark data are available, indicate that the pure RPA overestimates correlation energies and potentials as much as $E_c^{(2)}$.

One is therefore led to consider extensions of the RPA. The most obvious starting point for extension is the inclusion of the second order exchange (SOX) contribution. However, in its pure form it neglects the screening of the Coulomb interaction, which is the core feature of the RPA. One would thus expect an imbalance between direct and exchange contributions, when combining the RPA with the pure SOX term. A fully screened form of the SOX is easily formulated, following the line of thought used for the derivation of GGAs.⁴⁴ The resulting functional, however, is computationally much more demanding than the RPA. For that reason it is worthwhile to examine alternative modifications of the SOX term which reduce its net contribution. Given the success of the EN-resummation in the context of the complete $E_c^{(2)}$, an EN-extension of the SOX term suggests itself (this functional is denoted as RSOX in the following).

The SOX term, be it screened or not, is inherently a short-range contribution. This raises the question whether it is sufficient to account for the complete screened SOX in an approximate fashion, relying on the LDA. In fact, using this strategy, one can easily include all short-range correlation effects beyond the RPA.^{4,6} Clearly, the resulting LDA-type functional (here labeled as RPA+) is even more efficient than the RSOX.

In this work, we study the RPA and these simple extensions for a series of prototype atoms and ions, for which highly accurate reference data are available for comparison. In order to provide benchmark results a numerically exact, i.e., basis-set-free, approach is used and considerable emphasis is placed on all convergence issues involved. As a by-product of this strive for accuracy, a highly efficient scheme for performing the frequency integration inherent in all RPA-type functionals has been developed. This procedure should be useful for applications to more complex systems, for which utilizing more than the minimum number of grid points for the frequency integration would be too demanding.

A complete implementation of any XC functional requires not only the evaluation of the XC energy, but also the inclusion of the corresponding XC potential v_{xc} in the self-

consistent calculation. The latter step is quite challenging in the case of orbital-dependent XC functionals, for which v_{xc} has to be determined indirectly via the optimized potential method (OPM),^{25-28,30} and, in particular, for RPA-type functionals.^{35,38,45-50} Recently, Hellgren and von Barth have reported the first self-consistent RPA correlation potentials for spherical atoms, obtained by solution of the linearized Sham-Schluter equation⁵¹ at the GW level.⁴³ However, as indicated earlier, the RPA is not consistently improving atomic correlation potentials over $E_c^{(2)}$. In the present work we therefore focus on the perturbative evaluation of all RPA-type energies, utilizing self-consistent exchange-only orbitals and eigenvalues. As we will show, the RPA correlation energy is rather insensitive to the KS orbitals used for its evaluation, which clearly supports this perturbative approach. This feature, if true in general, will be very important for the application of RPA-type functionals to more complicated systems, for which a self-consistent implementation is not feasible anyway.

The paper is organized as follows. In the Sec. II, first the RPA correlation energy is formulated in the framework of the ACFD formalism. In addition, the general result is reduced to an expression valid for spherical systems. In Sec. III, various numerical aspects are discussed, addressing, in particular, questions of accuracy. In Sec. IV, the RPA correlation energies for a number of prototype atoms and ions (we will no longer distinguish between neutral atoms and atomic ions in the following) are presented and compared to the corresponding exact data. Section V provides a summary. Atomic units are used throughout this paper.

II. THEORY

A. RPA correlation energy on basis of the ACFD formalism

Based on the adiabatic connection and the zero-temperature fluctuation-dissipation theorem,^{42,52} the exact KS correlation energy can be written as

$$E_c = -\frac{1}{2\pi} \int_0^\infty du \int_0^1 d\lambda \int d\mathbf{r} d\mathbf{r}' v_{ee}(\mathbf{r} - \mathbf{r}') \times [\chi_\lambda(\mathbf{r}, \mathbf{r}', iu) - \chi_0(\mathbf{r}, \mathbf{r}', iu)], \quad (1)$$

where $v_{ee}(\mathbf{r}, \mathbf{r}') = 1/|\mathbf{r} - \mathbf{r}'|$ is the bare Coulomb interaction, χ_0 is the KS response function,

$$\chi_0(\mathbf{r}, \mathbf{r}', iu) = \sum_{ia} \frac{\phi_i^\dagger(\mathbf{r}) \phi_a(\mathbf{r}) \phi_a^\dagger(\mathbf{r}') \phi_i(\mathbf{r}')}{iu + \varepsilon_i - \varepsilon_a} + \text{c.c.}, \quad (2)$$

and χ_λ , with $\lambda \in [0, 1]$, is the density-density response function of a fictitious system in which electrons interact with a scaled Coulomb potential $\lambda v_{ee}(\mathbf{r}, \mathbf{r}')$, and simultaneously move in a modified external potential, chosen such that the electron density remains identical to that of the fully interacting system with $\lambda=1$. Throughout this paper we use the convention that i, j, \dots denote occupied (hole) KS states, while a, b, \dots are used for unoccupied (particle) states, and p, q, \dots for the general case. χ_λ is related to χ_0 by a Dyson-type integral equation,⁵³

$$\chi_\lambda(\mathbf{r}, \mathbf{r}', i\omega) = \chi_0(\mathbf{r}, \mathbf{r}', i\omega) + \int d\mathbf{r}_1 \int d\mathbf{r}_2 \chi_0(\mathbf{r}, \mathbf{r}_1, i\omega) \times K_\lambda(\mathbf{r}_1, \mathbf{r}_2, i\omega) \chi_\lambda(\mathbf{r}_2, \mathbf{r}', i\omega), \quad (3)$$

where

$$K_\lambda(\mathbf{r}_1, \mathbf{r}_2, i\omega) = \lambda v_{ee}(\mathbf{r}_1, \mathbf{r}_2) + f_{xc}^\lambda(\mathbf{r}_1, \mathbf{r}_2, i\omega) \quad (4)$$

is the Coulomb and XC kernel.

The RPA correlation energy is obtained from Eq. (1) if one neglects the XC contribution to the right-hand side of Eq. (3). Integrating over λ one ends up with

$$E_c^{\text{RPA}} = \int_0^\infty \frac{d\omega}{2\pi} \text{Tr} \{ \ln(1 - \chi_0(i\omega)v_{ee}) + \chi_0(i\omega)v_{ee} \}, \quad (5)$$

where the trace indicates integration over all spatial coordinates. It is often more instructive to rewrite the integrand in Eq. (5), denoted as $E_c(i\omega)$, as a power series in the Coulomb interaction,

$$E_c(i\omega) = - \sum_{n=2}^{\infty} \frac{1}{n} \text{Tr} \{ (\chi_0(i\omega)v_{ee})^n \}. \quad (6)$$

B. Correlation energy beyond RPA

The ACFD theorem provides a natural starting point for the development of correlation functionals beyond the RPA: Inclusion of some approximation for f_{xc} in the Dyson equation [Eq. (3)] automatically yields an extension of the RPA. Several approximate XC kernels have been introduced in the context of time-dependent DFT (TDDFT).^{54,55} It is, however, not clear whether an approximate f_{xc} designed to provide a good description of excited states within TDDFT also leads to accurate ground state correlation energies.

A more straightforward extension of the RPA, the so-called RPA+ approach, had been proposed by Kurth and co-workers *et al.*^{4,6} They observed that the RPA provides a quite accurate description of long-range correlation, but is inadequate for short-range correlations. On the other hand, the latter can be very well approximated by a local or semilocal density-based functional (LDA- or GGA-type),

$$E_c^{\text{RPA+}} = E_{c,\text{sr}}^{\text{LDA}} + E_c^{\text{RPA}}, \quad (7)$$

where the LDA for the short-range contribution $E_{c,\text{sr}}$ can be obtained by subtraction of the RPA-limit from the full LDA correlation energy,

$$E_{c,\text{sr}}^{\text{LDA}} = E_c^{\text{LDA}} - E_c^{\text{LDA-RPA}}. \quad (8)$$

This approach is supported by the fact that the gradient correction to the short-range correlation is much smaller than that to the complete correlation energy.⁴ Though the RPA+ functional has been used recently to describe the interlayer dispersion interaction in boron nitride,¹⁷ a direct comparison of the RPA+ with exact results is still missing even for closed-shell atoms. Using numerically exact RPA correlation energy available for atoms, we are able to give a unambiguous assessment of the quality of the RPA+ correlation functional.

In the language of Feynman diagrams, the RPA correlation energy is obtained from the second order direct diagram by replacing the bare Coulomb interaction by the dynamically screened Coulomb interaction. The dominant contribution that is missing in the RPA is the SOX diagram,

$$E_c^{\text{SOX}} = - \frac{1}{2} \sum_{ij,ab} \frac{(ij \parallel ab)(ab \parallel ji)}{\varepsilon_i + \varepsilon_j - \varepsilon_a - \varepsilon_b}, \quad (9)$$

where the notation

$$(pq \parallel rs) = \int d^3r \int d^3r' \frac{\phi_p^\dagger(\mathbf{r})\phi_r(\mathbf{r})\phi_q^\dagger(\mathbf{r}')\phi_s(\mathbf{r}')}{|\mathbf{r} - \mathbf{r}'|} \quad (10)$$

has been used for the KS Slater integral. Combining the RPA with the SOX term, one obtains a new functional, denoted as RPA+SOX. However, one would expect the SOX to overcorrect the error in the RPA, since the Coulomb interaction enters the SOX term in its bare, i.e., un-screened, form. Screening can be introduced into the SOX term in a systematic way by use of the same, dynamically screened interaction as in the direct term.⁴⁴ Unfortunately, the resulting functional is computationally much more demanding than the RPA expression. A technically much simpler way to reduce the SOX contribution has been suggested in the context of the second order functional $E_c^{(2)}$.^{39,56} The inclusion of the direct hole-hole contribution to the Epstein-Nesbet-type ladder diagrams into the SOX term substantially improves second order energies and potentials, without introducing any additional computational effort. Although the physical background of these ladder diagrams is quite different from dynamical screening, it seems worthwhile to analyze this “effective” screening. The resulting correction will be denoted as RSOX,

$$E_c^{\text{RSOX}} = - \frac{1}{2} \sum_{i,j,a,b} \frac{(ij \parallel ab)(ab \parallel ji)}{\varepsilon_i + \varepsilon_j - \varepsilon_a - \varepsilon_b - (ij \parallel ij)}. \quad (11)$$

C. RPA correlation functional for spherical systems

In the case of spherical systems, the KS potential only depends on the radial coordinate r , $v_s(\mathbf{r}) = v_s(r)$, and each KS orbital can be written as the product of a radial orbital and a spherical harmonic $Y_{lm}(\theta, \varphi)$,

$$\phi_k(\mathbf{r}) \rightarrow \phi_{nlm}(\mathbf{r}) = \frac{P_{nl}(r)}{r} Y_{lm}(\theta, \varphi), \quad (12)$$

where n , l , and m are the principle, angular, and magnetic quantum numbers, respectively. The P_{nl} are solutions of the radial KS equation,

$$\left[- \frac{1}{2} \left(\frac{d^2}{dr^2} - \frac{l(l+1)}{r^2} \right) + v_s(r) \right] P_{nl}(r) = \varepsilon_{nl} P_{nl}(r). \quad (13)$$

Two-body functions such as the Coulomb interaction and χ_0 can also be decomposed according to the spherical symmetry. To simplify notations, we use the following decomposition convention. The Coulomb interaction is expanded as

$$v_{\text{ce}}(\mathbf{r}, \mathbf{r}') = \sum_{L=0}^{\infty} \frac{4\pi}{2L+1} v_L(r, r') \sum_{M=-L}^L Y_{LM}(\theta, \varphi) Y_{LM}^*(\theta', \varphi'), \quad (14)$$

where

$$v_L(r, r') := r_{<}^L / r_{>}^{L+1}, \quad (15)$$

with $r_{<} = \text{Min}(r, r')$ and $r_{>} = \text{Max}(r, r')$. The response function χ_0 can be written as

$$\chi_0(\mathbf{r}, \mathbf{r}', iu) = \sum_{L=0}^{\infty} \frac{2L+1}{4\pi} \frac{\chi_{0L}(r, r', iu)}{r^2 r'^2} \sum_{M=-L}^L Y_{LM}(\theta, \varphi) Y_{LM}^*(\theta', \varphi'). \quad (16)$$

The L -dependent radial response function $\chi_{0L}(r, r', iu)$ can be calculated utilizing the radial orbitals,

$$\chi_{0L}(r, r', iu) = - \sum_{i\alpha\sigma} C_{L;i\alpha\sigma} D_{i\alpha\sigma}(iu) \Phi_{i\alpha\sigma}(r) \Phi_{i\alpha\sigma}(r'), \quad (17)$$

where

$$C_{L;i\alpha\sigma} := \frac{(2l_i+1)(2l_a+1)}{2L+1} \begin{pmatrix} l_i & l_a & L \\ 0 & 0 & 0 \end{pmatrix}^2, \quad (18)$$

$$D_{i\alpha\sigma}(iu) := \frac{2(\varepsilon_{a\sigma} - \varepsilon_{i\sigma})}{u^2 + (\varepsilon_{a\sigma} - \varepsilon_{i\sigma})^2}, \quad (19)$$

$$\Phi_{i\alpha\sigma}(r) := P_{i\sigma}(r) P_{a\sigma}(r). \quad (20)$$

Using the multipole expansion of both v_{ce} and χ_0 , the building block of the RPA correlation energy $\text{Tr}\{\chi_0 v\}$ is obtained as

$$\text{Tr}\{\chi_0 v\} = \sum_L (2L+1) \int_0^\infty dr dr' \chi_{0L}(r, r', iu) v_L(r', r). \quad (21)$$

There are two options for the calculation of the radial integral in Eq. (21).

1. Real space approach

In this approach, $\chi_{0L}(r, r')$ is calculated on a discrete radial mesh, which allows to evaluate Eq. (21) by direct numerical integration,

$$\begin{aligned} \text{Tr}\{\chi_0 v\} &= \sum_L (2L+1) \sum_{i,j} w(r_i) w(r_j) \chi_{0L}(r_i, r_j) v_L(r_j, r_i) \\ &= \sum_L (2L+1) \sum_{i,j} [\tilde{\chi}_{0L}]_{i,j} [v_L]_{j,i} \\ &= \sum_L (2L+1) \text{Tr}\{\tilde{\chi}_{0L} v_L\}, \end{aligned} \quad (22)$$

where w_i denotes the radial integral weight at mesh point i . In case of powers of $\text{Tr}\{\chi_0 v\}$ one has

$$\text{Tr}\{(\chi_0 v)^n\} = \sum_L (2L+1) \text{Tr}\{(\tilde{\chi}_{0L} v_L)^n\}. \quad (23)$$

The sum over n in Eq. (6) then leads to

$$E_c(iu) = \sum_L (2L+1) \text{Tr}\{\ln(1 - \tilde{\chi}_{0L} v_L) + \tilde{\chi}_{0L} v_L\}. \quad (24)$$

2. Orbital-product space approach

In this second approach one inserts Eqs. (16) and (17) into Eq. (21). Using the radial Slater integrals

$$R_{L;i\alpha\sigma,jb\sigma'} := \int_0^\infty dr \int_0^\infty dr' \Phi_{i\alpha\sigma}(r) v_L(r, r') \Phi_{jb\sigma'}(r'), \quad (25)$$

one finds

$$\begin{aligned} \text{Tr}\{\chi_0 v\} &= \sum_L (2L+1) \sum_{i\alpha\sigma} C_{L;i\alpha\sigma} D_{i\alpha\sigma}(iu) \\ &\quad \times \int dr \int dr' \Phi_{i\alpha\sigma}(r) v_L(r, r') \Phi_{i\alpha\sigma}(r') \\ &= - \sum_L (2L+1) \sum_{i\alpha\sigma} C_{L;i\alpha\sigma} D_{i\alpha\sigma}(iu) R_{L;i\alpha\sigma,i\alpha\sigma}. \end{aligned} \quad (26)$$

With the definitions

$$V_{L;i\alpha\sigma,jb\sigma'} := \sqrt{C_{L;i\alpha\sigma}} R_{L;i\alpha\sigma,jb\sigma'} \sqrt{C_{L;jb\sigma'}}, \quad (27)$$

$$S_{L;i\alpha\sigma,jb\sigma'} := - \sqrt{D_{i\alpha\sigma}(iu)} V_{L;i\alpha\sigma,jb\sigma'} \sqrt{D_{jb\sigma'}(iu)}, \quad (28)$$

one ends up with

$$\text{Tr}\{\chi_0 v\} = \sum_L (2L+1) \sum_{i\alpha\sigma} S_{L;i\alpha\sigma,i\alpha\sigma} = \sum_L (2L+1) \text{Tr}\{S_L\}. \quad (29)$$

One can furthermore show that

$$\text{Tr}\{(\chi_0 v)^n\} = \sum_L (2L+1) \text{Tr}\{(S_L)^n\}, \quad (30)$$

so that

$$\begin{aligned} E_c(iu) &= - \sum_L (2L+1) \text{Tr} \left\{ \sum_{n=2}^{\infty} \frac{(S_L)^n}{n} \right\} \\ &= \sum_L (2L+1) \text{Tr}[\ln(1 - S_L) + S_L] \\ &= \sum_L (2L+1) [\ln(\text{Det}(1 - S_L)) + \text{Tr}\{S_L\}]. \end{aligned} \quad (31)$$

The final expressions for E_c^{RPA} are quite similar in the real-space and orbital-product-space approaches, but their numerical efficiency can be very different, depending on the size of the system. In the real-space approach, the dimension of the matrix involved is determined by the number of mesh points used for radial integration, I_{max} . As I_{max} is never larger than a few thousand even for heavy atoms, the resulting memory requirement is quite low. On the other hand, χ_{0L} needs to be constructed on the radial mesh for each frequency, which can be very cpu-time-intensive. The situation is quite different in the case of the orbital-product space ap-

TABLE I. Convergence of E_c^{RPA} , the exact exchange energy, and the eigenvalue of the highest occupied KS orbital ($\varepsilon_{\text{HOMO}}$) obtained by self-consistent exchange-only calculations for Ar for different cavity radii R_{max} (with $n_{\text{max}}/R_{\text{max}}=10$ bohrs $^{-1}$, $l_{\text{max}}=4$, R_{max} in bohrs, and all energies are in hartree).

R_{max}	$-E_c^{\text{RPA}}$	$-E_x$	$\varepsilon_{\text{HOMO}}$
5	1.0023	30.2059	0.5772
8	1.0027	30.1749	0.5909
10	1.0028	30.1747	0.5908

proach. Here the dimension of the matrix involved is given by $N_{\text{occ}}N_{\text{vir}}$, where N_{occ} denotes the number of occupied orbitals and N_{vir} is the number of unoccupied orbitals taken into account. $N_{\text{occ}}N_{\text{vir}}$ can be easily as high as tens of thousands. However, the matrix V_L [Eq. (27)] is independent of frequency and can be calculated in advance and stored in the memory. Limitations of the available memory can be circumvented by taking advantage of the fact that, for given L , V_L and S_L are quite sparse (usually the ratio of nonzero elements is less than 1%). One can therefore use standard sparse matrix techniques to reduce the storage requirement and accelerate the computation of the determinant.

III. NUMERICAL DETAILS

A. Hard-wall cavity approach

The RPA correlation energy depends on the occupied as well as on the unoccupied KS states. For free atoms, the spectrum of the unoccupied states includes both discrete Rydberg states and continuum states. However, the handling of continuum states in the evaluation of the correlation energy is nontrivial.⁵⁷ Moreover, the presence of continuum states causes additional problems in the context of orbital-dependent functionals: One does no longer find a solution of the corresponding OPM equation which satisfies the standard boundary conditions for the correlation potential.⁵⁸ To resolve this problem, we developed a hard-wall cavity approach,^{38,56,58} in which the KS equation is solved on a discrete radial mesh with hard-wall boundary conditions imposed at a finite but large radius R_{max} . The same approach is used in the present work.

Its crucial parameters are the cavity radius R_{max} as well as the energetically highest state (characterized by its principle quantum number n_{max}) and the highest angular momentum l_{max} included in sums over virtual states. In the following, neutral Ar is used for a systematic convergence study with respect to R_{max} , n_{max} , and l_{max} .

We first consider R_{max} . R_{max} has to be chosen so large, that all ground state properties, and, in particular, the correlation energy, do no longer change when R_{max} is increased further. However, any increase of R_{max} directly affects the spectrum of the positive energy states, i.e., the density of states. In order to keep the space available for virtual excitations constant, when increasing R_{max} , one therefore has to fix the energy ε_{max} of the highest unoccupied state n_{max} taken into account. In the case of very high-lying virtual states one

TABLE II. Convergence of full E_c^{RPA} (Column 3) and E_c^{RPA} within the frozen core approximation excluding virtual excitations of the $1s$, $2s$, and $2p$ electrons (Column 4) of Ar with respect to n_{max} (with $R_{\text{max}}=10$ bohrs, $l_{\text{max}}=4$, and all energies are in hartree).

n_{max}	ε_{max}	$-E_c^{\text{RPA}}$	$-E_c^{\text{RPA}}$ (FC)
25	25.1	0.6840	0.3961
50	111.9	0.9097	0.3980
100	471.2	1.0028	0.3980
150	1077.6	1.0273	0.3980
200	1930.8	1.0354	0.3980
250	3030.9	1.0384	0.3980
300	4377.6	1.0398	0.3980
350	5951.9	1.0399	0.3980
400	7754.8	1.0400	0.3980

has a simple relation between R_{max} and ε_{max} , resulting from the fact that high-lying states are no longer sensitive to the detailed structure of v_s ,

$$\varepsilon_{\text{max}} \propto \left(\frac{n_{\text{max}}}{R_{\text{max}}} \right)^2. \quad (32)$$

The space available for virtual excitations is therefore kept constant, as soon as the ratio $n_{\text{max}}/R_{\text{max}}$ is fixed. Table I shows the values of E_c^{RPA} for Ar obtained with different R_{max} , but fixed $n_{\text{max}}/R_{\text{max}}=10$ bohrs $^{-1}$, which corresponds to an energy cut-off of about 500 hartree. For comparison, the corresponding exchange energy and the eigenvalue of the highest occupied orbital $\varepsilon_{\text{HOMO}}$ resulting from exchange-only calculations are also listed. One observes that E_c^{RPA} is less sensitive to R_{max} than the exchange energy, which is consistent with the fact that the length scale related to the RPA correlation energy is smaller compared to that of the exchange.

Argon is the heaviest atom considered in this work. We have also made systematic convergence tests for other less compact atoms such as Na and Mg. For all atoms considered in this work, the choice $R_{\text{max}}=10$ bohrs leads to errors less than 1 mhartree.

With R_{max} fixed, one can now examine the convergence of E_c^{RPA} with respect to n_{max} and l_{max} . Tables II and III show E_c^{RPA} for Ar obtained with different n_{max} and l_{max} . In general, the absolute value of E_c^{RPA} converges quite slowly with respect to both parameters. The slow convergence with respect

TABLE III. Convergence of full E_c^{RPA} (Column 3) and E_c^{RPA} within the frozen core approximation excluding virtual excitations of the $1s$, $2s$, and $2p$ electrons (Column 4) of Ar with respect to l_{max} (with $R_{\text{max}}=10$ bohrs, and $n_{\text{max}}=100$, and all energies are in hartree).

l_{max}	$-E_c^{\text{RPA}}$	$-E_c^{\text{RPA}}$ (FC)
2	0.7661	0.2875
4	1.0028	0.3980
6	1.0431	0.4185
8	1.0529	0.4241
10	1.0562	0.4262
12	1.0574	0.4271
14	1.0580	
16	1.0582	

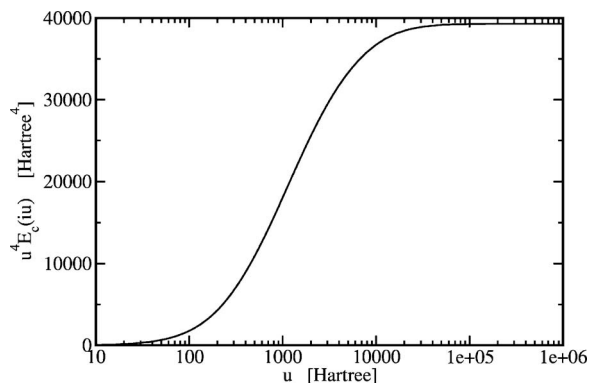


FIG. 1. $u^4 E_c(iu)$ vs u for He (maximum excitation energy $\delta\epsilon \approx 4000$ hartree).

to n_{\max} mainly originates from the innermost shell—unoccupied states with high energies are only important for the description of virtual excitations of the highly localized, low-lying core states. In practice, fortunately only energy differences related to the valence electrons are really relevant. One would thus expect to achieve high accuracy for these energy differences with much more moderate values for n_{\max} . This suggests to rely on the frozen core (FC) approximation, in which excitations from core levels are excluded. Tables II and III demonstrate that the FC approximation for E_c^{RPA} converges much faster with increasing n_{\max} . Even for a quite moderate n_{\max} of 25, corresponding to $\epsilon_{\max} \sim 25$ hartree, E_c^{RPA} is already converged to an accuracy of 2 mhartree. On the other hand, the convergence behavior of E_c^{RPA} with respect to l_{\max} is not improved by the FC approximation. As one of the main aims of this work is to provide benchmark results for a set of prototype atoms, most results reported in this work are obtained without evoking the FC approximation. The results reported in the next section are obtained for $n_{\max}=300$ and $l_{\max}=14$, which ensures an accuracy of 1 mhartree for Ar and better for all lighter atoms.

B. Frequency integration

Any calculation of RPA energies involves two time-consuming steps: The first is the evaluation of all Slater integrals involved, i.e., of the matrix R_L , Eq. (25). In the present work the Slater integrals are calculated by numerical integration on the radial grid, using standard finite differences methods. Once R_L is available, the second step is performing the frequency integration in Eq. (5). In order to understand the most appropriate way to do this frequency integration is for us to consider the integrand for some prototype atoms. Figure 1 shows $u^4 E_c(iu)$ for He, demonstrating the fact that $E_c(iu)$ falls off as u^{-4} for extremely large u .

This behavior can be easily understood on the basis of Eq. (19): For frequencies beyond the maximum excitation energy $\delta\epsilon = \epsilon_{a\sigma}^{\max} - \epsilon_{i\sigma}$ included in the calculation (or provided by the basis set) $D_{ia\sigma}(u)$ and thus $S_L(u)$ decay as u^{-2} which allows a perturbative evaluation of Eq. (31) in powers of $S_L(u)$, with the second order term dominating the resulting $E_c(iu)$.

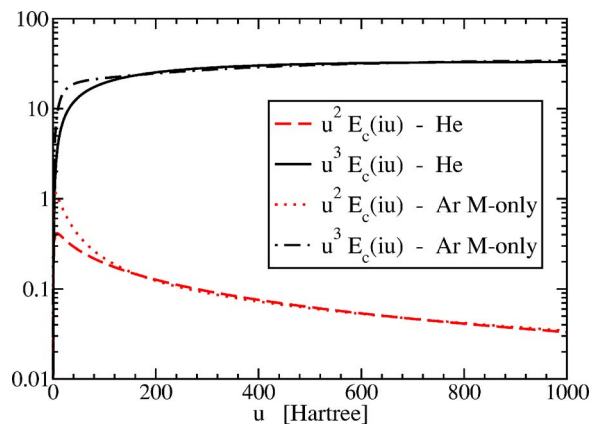


FIG. 2. (Color online) $u^2 E_c(iu)$ and $u^3 E_c(iu)$ vs u for moderately large u for the case of He.

On the other hand, for the more important range of large frequencies less than $\delta\epsilon$ a decay close to u^{-3} is found, as shown in Fig. 2.

The same behavior is observed for each individual shell, as illustrated by the $E_c(iu)$ obtained by excitation of only the M -shell of neutral Ar, also included in Fig. 2.

This power law decay suggests a transformation of the frequency interval $0 \leq u < \infty$ to some finite interval via a power law transformation, as, for instance,

$$x = \frac{1}{1 + (u/s)} \quad 0 \leq x \leq 1, \quad (33)$$

giving more weight to large u than an exponential transformation. The scale factor s is intrinsically related to the minimum energy required for a virtual excitation, which is roughly given by the eigenvalue difference $\epsilon_{\text{LUMO}} - \langle \epsilon \rangle \approx |\langle \epsilon \rangle|$ for a shell with average eigenvalue $\langle \epsilon \rangle$. The most appropriate s can only be determined empirically. For all atoms considered in detail the choice $s=2|\langle \epsilon \rangle|$ seemed to work reasonably well (see also below). The result of the transformation [Eq. (33)] is shown in Fig. 3 for He, Ar¹⁶⁺, as well as the M -shell of neutral Ar.

One obtains a smooth function of x , with values remain-

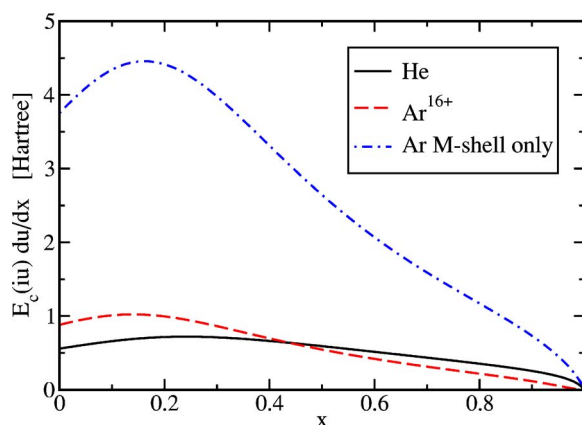
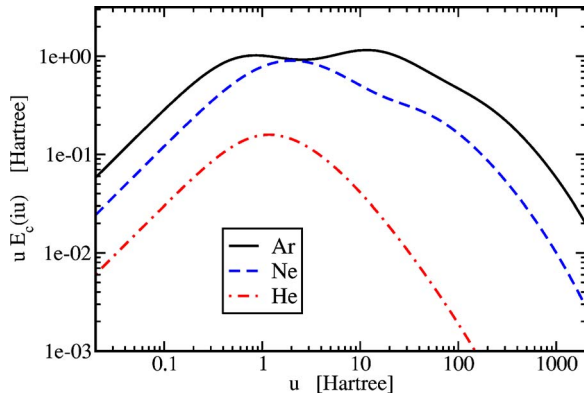


FIG. 3. (Color online) Integrand $E_c(iu) du/dx$ of frequency integral after the transformation [Eq. (33)] vs x for He, Ar¹⁶⁺, as well as the M -shell of neutral Ar.

FIG. 4. (Color online) $uE_c(iu)$ vs u for He, Ne and Ar.

ing on the same order of magnitude for all x . This ensures a rapid convergence of the numerical integration over x with the number of grid points.

However, the frequency integration in Eq. (5) suffers from the fact that each shell in an atom (or molecule) introduces a new energy scale for the virtual excitations. This is most easily verified by plotting $uE_c(iu)$ on a double logarithmic scale, as done in Fig. 4 for He, Ne, and Ar.

Figure 4 demonstrates that there are two relevant scales for Ne and three in the case of Ar. In fact, the plots confirm that the behavior of $E_c(iu)$ changes at roughly twice the average eigenvalues of the shells involved, with the position of the highest energy transition point being somewhat less pronounced [$\epsilon_K(\text{Ne})=-30.8$ and $\epsilon_L(\text{Ne})=-1.1$ and $\epsilon_K(\text{Ar})=-114.4$, $\epsilon_L(\text{Ar})=-9.4$, and $\epsilon_M(\text{Ar})=-0.7$, which are all values in hartree]. It is therefore necessary to split the frequency integration from 0 to ∞ into intervals associated with these individual energy scales. Let us call the boundaries of the intervals b_i ,

$$0 = b_0 < b_1 < \dots < b_n = \infty, \quad (34)$$

with n denoting the number of shells. The intervals are chosen such that the characteristic energy scale s_n of shell n is bracketed,

$$b_{i-1} < s_i < b_i. \quad (35)$$

In practice, $s_i = 2|\langle \epsilon_i \rangle|$ and $b_i = 4|\langle \epsilon_i \rangle|$ seemed to provide a reasonable partitioning of the complete frequency range. Equation (5) may then be decomposed as

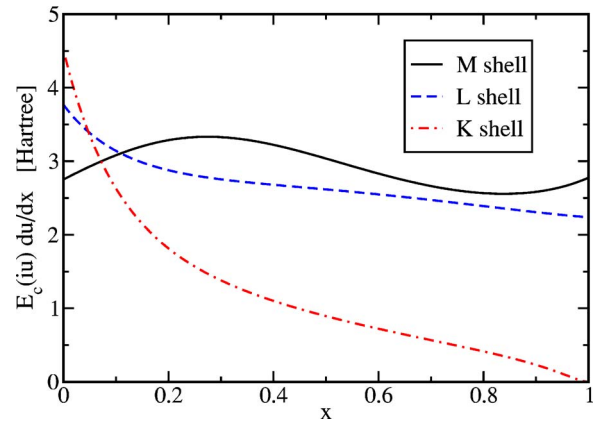
$$\int_0^\infty E_c(iu) du = \sum_{i=1}^n \int_{b_{i-1}}^{b_i} E_c(iu) du. \quad (36)$$

In order to account for the piecewise decay of $E_c(iu)$ the transformation

$$x_i = \frac{[1 + s_i/(b_i - b_{i-1})]u - b_{i-1}}{[1 + (u - b_{i-1})/s_i] s_i} \quad (37)$$

$$\frac{du}{dx_i} = s_i \frac{[1 + s_i/(b_i - b_{i-1})]}{[1 + s_i/(b_i - b_{i-1}) - x_i]^2} \quad (38)$$

($i=1, \dots, n$) is most suitable. Equation (36) can then be written as

FIG. 5. (Color online) Integrand $E_c(iu(x))du/dx$ of partitioned frequency integral [Eq. (39)] resulting from the transformation [Eq. (37)] for neutral Ar.

$$\int_0^\infty E_c(iu) du = \sum_{i=1}^n \int_{-1}^1 dx_i \frac{du}{dx_i} E_c(iu(x_i)). \quad (39)$$

The success of this frequency partitioning plus the power law transformation scheme is demonstrated in Fig. 5, in which the final integrands $du/dx_i E_c(iu(x_i))$ are plotted for neutral Ar.

In all three energy regimes a rather smooth integrand is obtained, which allows the application of a Gauss-Legendre quadrature to each interval. As a result, the error obtained for a given total number of grid points N_u used for the Gauss-Legendre quadrature is rather small already for very low N_u , as illustrated in Fig. 6.

The most critical interval in Eq. (39) is the highest energy range, covering, in particular, excitations of the $1s$ -state. For that reason the error is even lower if only excitations of the valence shell are included (i.e., in the FC approximation), as is obvious from the error found for He or the M -shell of neutral Ar.

IV. RESULTS

A. Sensitivity to form of KS orbitals

Standard KS-DFT calculations are based on the self-consistent solution of the KS equations, which requires the

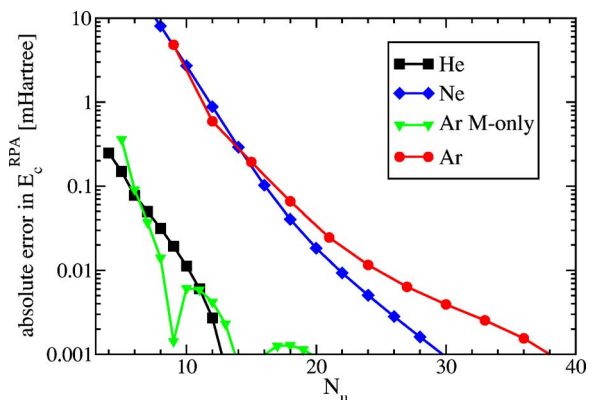
FIG. 6. (Color online) Absolute error resulting from Eqs. (39) and (37) as a function the total number of grid points N_u used for the Gauss-Legendre quadrature (note that N_u is the sum of the number of grid points used in the individual intervals).

TABLE IV. Absolute RPA total energies (in hartree) resulting from insertion of different KS orbitals. The last row lists the self-consistent RPA total energies given in Ref. 43.

KS orbitals	He	Be	Ne	Mg	Ar	N	Na
LDA	2.945	14.751	129.140	200.293	527.905	54.735	162.475
BLYP	2.944	14.752	129.142	200.296	527.910	54.737	162.478
EXX-only	2.945	14.752	129.143	200.298	527.913	54.738	162.480
RPA	2.945	14.754	129.143	200.296	527.908

evaluation of the XC potential $v_{xc}(\mathbf{r}) = \delta E_{xc}[n] / \delta n(\mathbf{r})$. In the case of LDA and GGA functionals the calculation of $v_{xc}(\mathbf{r})$ is straightforward. On the other hand, a self-consistent implementation represents a much more serious problem for RPA-type functionals. First of all, in the case of orbital-dependent functionals v_{xc} has to be determined via the OPM, i.e., by solution of an integral equation.³⁰ The solution of the OPM integral equation is well-established for the exact exchange and manageable, though rather intricate, for the second order correlation functional $E_c^{(2)}$.^{36-38,59} Its implementation for RPA-type functionals, however, is much more challenging, so that a full solution has only been reported very recently.⁴³ On the other hand, a self-consistent implementation is only then advantageous if the resulting correlation potential leads to an improved total KS potential. It has been demonstrated that this is not the case for some standard GGAs (Ref. 60) and for $E_c^{(2)}$,^{38,39} which by far overestimates correlation effects. The situation is not yet completely clear in the case of the RPA. The first RPA potentials available⁴³ seem to improve over $v_c^{(2)} = \delta E_c^{(2)} / \delta n(\mathbf{r})$ in the asymptotic regime, but otherwise often follow $v_c^{(2)}$.

Independently of this more fundamental aspect, one might ask whether a self-consistent implementation is really necessary to obtain accurate RPA correlation and thus ground state energies. Clearly, a purely perturbative treatment of RPA-type functionals on the basis of a self-consistent calculation with the exact exchange would allow their application to much more complex systems, for which the solution of the corresponding OPM integral equation is beyond current computer resources. In fact, our experience with conventional density functionals suggests that, at least for atomic systems, the RPA correlation energy is not sensitive to the detailed structure of $v_{xc}(\mathbf{r})$.

In order to verify this expectation, the RPA ground state energy (i.e., the sum of the KS kinetic energy, the Hartree term, the exact exchange and E_c^{RPA}) has been calculated by insertion of KS orbitals resulting from different XC functionals: Orbitals obtained from self-consistent calculations with only the exact exchange (EXX-only), but neglecting v_c completely, are compared with self-consistent LDA and GGA orbitals. The results for a number of atoms are collected in Table IV, which also includes recent self-consistent RPA energies,⁴³ whenever available. Table IV confirms the expectation: Even though the KS potentials obtained by EXX-only calculations differ substantially from their LDA and GGA counterparts, the differences between the resulting RPA energies are quite small. The same is true for the deviations between the perturbative RPA energies on EXX-only basis

TABLE V. Absolute correlation energies (in hartree) of closed subshell atoms calculated from the RPA and RPA+ functionals by insertion of the exact EXX-only KS orbitals in comparison with exact data Ref. (62). The last row provides the mean absolute error (MAE) with respect to the exact energies.

Atom	Exact	RPA	RPA+	RPA+SOX	RPA+RSOX	LYP
He	0.042	0.083	0.047	0.035	0.044	0.044
Li ⁺	0.043	0.087	0.048	0.039	0.045	0.048
Be ²⁺	0.044	0.088	0.048	0.041	0.045	0.049
Li	0.045	0.112	0.059	0.029	0.053	0.053
Be ⁺	0.047	0.122	0.066	0.031	0.056	0.061
B ²⁺	0.049	0.131	0.073	0.030	0.059	0.067
Be	0.094	0.179	0.108	0.058	0.097	0.095
B ⁺	0.111	0.205	0.131	0.066	0.110	0.107
C ²⁺	0.126	0.228	0.151	0.073	0.123	0.114
N	0.188	0.335	0.201	0.146	0.178	0.192
O ⁺	0.194	0.345	0.208	0.155	0.184	0.207
F ²⁺	0.199	0.355	0.215	0.162	0.189	0.218
Ne	0.390	0.597	0.400	0.340	0.367	0.384
Na ⁺	0.389	0.599	0.398	0.350	0.371	0.399
Mg ²⁺	0.390	0.601	0.398	0.358	0.375	0.411
Na	0.396	0.626	0.410	0.349	0.383	0.408
Mg ⁺	0.400	0.634	0.415	0.360	0.389	0.427
Al ²⁺	0.405	0.642	0.420	0.369	0.395	0.442
Mg	0.438	0.687	0.453	0.387	0.427	0.459
Al ⁺	0.452	0.706	0.468	0.402	0.440	0.481
Si ²⁺	0.463	0.722	0.481	0.414	0.451	0.497
P	0.540	0.850	0.554	0.482	0.523	0.566
S ⁺	0.556	0.873	0.573	0.499	0.538	0.588
Cl ²⁺	0.570	0.893	0.589	0.514	0.552	0.605
Ar	0.722	1.101	0.742	0.661	0.701	0.751
K ⁺	0.739	1.126	0.763	0.681	0.720	0.771
Ca ²⁺	0.754	1.150	0.783	0.702	0.737	0.788
MAE		0.196	0.015	0.039	0.011	0.018

and the self-consistent RPA results. This result is expected to hold quite generally, as long as one does not examine a quantity which is particularly sensitive to the correlation potential (as, for instance, the quantum defect of high Rydberg states⁶¹). In fact, Table IV indicates that even a perturbative treatment of both the exact exchange and the RPA may be legitimate for very complex systems, in which even self-consistent calculations with the exact exchange are too expensive. In the following sections, self-consistent EXX-only orbitals are always used for the evaluation of the RPA correlation energy.

B. RPA correlation energies of spherical atoms

In this work, we focus on atoms with closed or half-filled shells, for which the ground state KS potentials for the two spin-channels are both spherically symmetric. Table V lists the correlation energies obtained from all four RPA-based functionals for a series of atoms. To see trends more clearly, the relative errors resulting from the various functionals with respect to the exact correlation energies⁶² are plotted in Fig. 7. Not surprisingly, the pure RPA always overestimates the true correlation energy. Adding the short-range correction within the LDA (RPA+) improves the results remarkably, reducing the mean absolute error by more than an

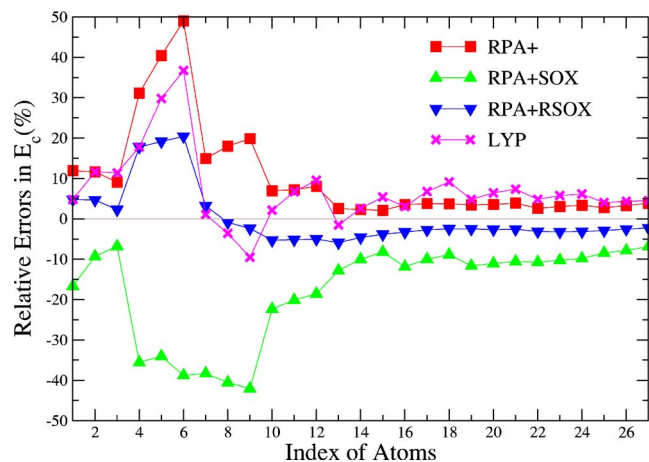


FIG. 7. (Color online) Relative errors resulting from different approximate correlation energies, obtained from the data in Table V.

order of magnitude. As expected, the unscreened SOX contribution by far overcorrects the error of the RPA. On the other hand, the inclusion of EN-corrections into the SOX term (RSOX) reduces this overcorrection significantly. In general, both the RPA+ and the RPA+RSOX produce more accurate correlation energies than the LYP-GGA, at least for the set of atoms considered in this work. Moreover, for light atoms one observes a tendency of the RPA+RSOX to be superior to the RPA+.

C. Ionization potentials

Even more important than the accuracy of total (correlation) energies is the accuracy of energy differences. In the case of atoms the ionization potential (IP) serves as the prototype energy difference for assessing the quality of any approximation. Much more than the total atomic E_c , the IP probes the description of the correlation of the valence states. We have therefore calculated the IPs resulting from the four RPA-based correlation functionals for a number of atoms. In order to avoid any uncertainty associated with spherical averaging, the comparison is restricted to atoms for which both the KS potential of the neutral ground state and that corresponding to the ionic state are spherical. The results are collected in Table VI. The most noteworthy features of these data are as follows: (1) The pure RPA, though showing significant improvement over the EXX-only approximation,

generally overestimates the true IPs; (2) correspondingly, the RPA+SOX underestimates IPs (consistent with the unscreened nature of the pure SOX term); (3) both the RPA+ and the RPA+RSOX significantly improve over the pure RPA results, and are even more accurate than BLYP, the “most accurate” standard GGA.

V. SUMMARY AND CONCLUSIONS

In this work, we provide benchmark results for the RPA and three simple extensions, allowing for an unambiguous assessment of the functionals by comparison with exact data. Our results confirm earlier observations of the limited applicability of the pure RPA: The RPA substantially overestimates correlation energies, which then results in an overestimation of energy differences such as ionization potentials. On the other hand, our results also demonstrate that already quite simple extensions of the RPA can be superior to standard GGAs: Adding either short-range corrections within the LDA (RPA+) or a suitably “screened” second order exchange contribution (RPA+RSOX) significantly improves both absolute energies and energy differences. This success is consistent with the expectation that the dominant source of error in the RPA functional is the missing short-range SOX contribution.

It seems worthwhile emphasizing that the first of these extensions, the RPA+, essentially comes at no cost: Compared to the computational demands of a RPA-calculation, the cost of the LDA for the non-RPA correlation is irrelevant. Moreover, a systematic improvement of the RPA+ by inclusion of gradient corrections for the non-RPA correlation contributions suggests itself. The RPA+RSOX involves an evaluation of the orbital-dependent SOX term, which is computationally almost as demanding as the calculation of the RPA energy itself, but is still much less expensive than that of the fully screened SOX term.

In this work also several technical aspects of RPA-calculations have been studied systematically, of which two should be relevant beyond the regime of atoms considered here. The first of these aspects is the sensitivity of the RPA-expression to the orbitals and eigenvalues used for its evaluation. It turned out that the character of the KS spectrum inserted into the RPA has little impact on the resulting energy. Even if KS states obtained by LDA calculations are

TABLE VI. First ionization potentials (in hartree) of spherical atoms calculated from total energy differences [$IP = E_{\text{tot}}(N-1) - E_{\text{tot}}(N)$], using different XC functionals. The last row provides the mean absolute error (MAE) with respect to the exact results (Ref. 62). Self-consistent EXX-only KS orbitals are used as input orbitals.

Atom	Exact	EXX	RPA	RPA+	RPA+SOX	RPA+RSOX	BLYP
Li	0.198	0.195	0.220	0.205	0.185	0.203	0.201
Be ⁺	0.669	0.666	0.700	0.683	0.656	0.677	0.681
Be	0.343	0.295	0.352	0.338	0.323	0.336	0.329
B ⁺	0.924	0.861	0.935	0.919	0.897	0.912	0.904
Na	0.189	0.179	0.206	0.191	0.178	0.191	0.194
Mg ⁺	0.552	0.540	0.573	0.557	0.543	0.555	0.566
Mg	0.281	0.242	0.294	0.279	0.268	0.279	0.279
Al ⁺	0.691	0.643	0.706	0.691	0.677	0.688	0.691
MAE		0.028	0.017	0.005	0.015	0.005	0.009

used the deviations from more accurate data remain small. In order to cover systems with more than one occupied shell, we have developed a partitioning scheme for the frequency integration inherent in all RPA-type functionals, which, together with a suitable transformation of the integration variable, allows to perform the frequency integration with a minimum number of mesh points. Both these numerical techniques should be particularly helpful for applications to more complex systems.

ACKNOWLEDGMENTS

Financial support by the Deutsche Forschungsgemeinschaft (Grant No. EN 265/4-2) is gratefully acknowledged. The calculations for this work have been performed on the computer cluster of the Center for Scientific Computing of J. W. Goethe-Universität Frankfurt.

- ¹J. F. Dobson, in *Topics in Condensed Matter Physics*, edited by M. P. Das (Nova, New York, 1994), Chap. 2, p. 121. See also F. Dobson, e-print arXiv:cond-mat/0311371.
- ²J. M. Pitarke and A. G. Eguiluz, *Phys. Rev. B* **57**, 6329 (1998).
- ³J. F. Dobson and J. Wang, *Phys. Rev. Lett.* **82**, 2123 (1999).
- ⁴S. Kurth and J. P. Perdew, *Phys. Rev. B* **59**, 10461 (1999).
- ⁵M. Lein, J. F. Dobson, and E. K. U. Gross, *J. Comput. Chem.* **20**, 12 (1999).
- ⁶Z. Yan, J. P. Perdew, and S. Kurth, *Phys. Rev. B* **61**, 16430 (2000).
- ⁷M. Lein, E. K. U. Gross, and J. P. Perdew, *Phys. Rev. B* **61**, 13431 (2000).
- ⁸J. F. Dobson and J. Wang, *Phys. Rev. B* **62**, 10038 (2000).
- ⁹F. Furche, *Phys. Rev. B* **64**, 195120 (2001).
- ¹⁰M. Fuchs and X. Gonze, *Phys. Rev. B* **65**, 235109 (2002).
- ¹¹T. Miyake, F. Aryasetiawan, T. Kotani, M. van Schilfgaarde, M. Usuda, and K. Terakura, *Phys. Rev. B* **66**, 245103 (2002).
- ¹²K. Fuchs, M. Burke, Y.-M. Niquet, and X. Gonze, *Phys. Rev. Lett.* **90**, 189701 (2003).
- ¹³J. M. Pitarke and J. P. Perdew, *Phys. Rev. B* **67**, 045101 (2003).
- ¹⁴J. Jung, P. Garcia-Gonzalez, J. F. Dobson, and R. W. Godby, *Phys. Rev. B* **70**, 205107 (2004).
- ¹⁵F. Furche and T. Voorhis, *J. Chem. Phys.* **122**, 164106 (2005).
- ¹⁶M. Fuchs, Y.-M. Niquet, X. Gonze, and K. Burke, *J. Chem. Phys.* **122**, 094116 (2005).
- ¹⁷A. Marini, P. Garcia-Gonzalez, and A. Rubio, *Phys. Rev. Lett.* **96**, 136404 (2006).
- ¹⁸P. Sánchez-Friera and R. W. Godby, *Phys. Rev. Lett.* **85**, 5611 (2000).
- ¹⁹P. Garcia-Gonzalez and R. W. Godby, *Phys. Rev. Lett.* **88**, 056406 (2002).
- ²⁰F. Aryasetiawan, T. Miyake, and K. Terakura, *Phys. Rev. Lett.* **88**, 166401 (2002).
- ²¹N. E. Dahlen and U. von Barth, *Phys. Rev. B* **69**, 195102 (2004).
- ²²N. E. Dahlen, R. van Leeuwen, and U. von Barth, *Phys. Rev. A* **73**, 012511 (2006).
- ²³R. G. Parr and W. Yang, *Density-Functional Theory of Atoms and Molecules* (Oxford University Press, New York, 1989).
- ²⁴R. M. Dreizler and E. K. U. Gross, *Density Functional Theory: An Approach to the Quantum Many-Body Problem* (Springer-Verlag, Berlin, 1990).
- ²⁵E. Engel and R. M. Dreizler, *J. Comput. Chem.* **20**, 31 (1999).
- ²⁶T. Grabo, T. Kreibich, S. Kurth, and E. K. U. Gross, in *Strong Coulomb Correlations in Electronic Structure Calculations: Beyond the Local Density Approximation*, edited by V. I. Anisimov (Gordon and Breach, New York, 1999), p. 203.
- ²⁷E. Engel, in *A Primer in Density Functional Theory*, edited by C. Fiolhais, F. Nogueira, and M. Marques (Springer, Berlin, 2003), Chap. 2, pp. 56–143.
- ²⁸A. Görling, *J. Chem. Phys.* **123**, 062203 (2005).
- ²⁹E. J. Baerends, *J. Chem. Phys.* **123**, 062202 (2005).
- ³⁰J. D. Talman and W. F. Shadwick, *Phys. Rev. A* **14**, 36 (1976).
- ³¹E. Engel, A. F. Bonetti, S. Keller, I. Andrejkovics, and R. M. Dreizler, *Phys. Rev. A* **58**, 964 (1998).
- ³²E. Engel, A. Höck, and R. M. Dreizler, *Phys. Rev. A* **61**, 032502 (2000).
- ³³L. J. Sham, *Phys. Rev. B* **32**, 3876 (1985).
- ³⁴A. Görling and M. Levy, *Phys. Rev. A* **50**, 196 (1994).
- ³⁵A. Facco Bonetti, E. Engel, R. N. Schmid, and R. M. Dreizler, *Phys. Rev. Lett.* **86**, 2241 (2001).
- ³⁶I. Grabowski, S. Hirata, S. Ivanov, and R. J. Bartlett, *J. Chem. Phys.* **116**, 4415 (2002).
- ³⁷P. Mori-Sanchez, Q. Wu, and W. Yang, *J. Chem. Phys.* **123**, 062204 (2005).
- ³⁸H. Jiang and E. Engel, *J. Chem. Phys.* **123**, 224102 (2005).
- ³⁹H. Jiang and E. Engel, *J. Chem. Phys.* **125**, 184108 (2006).
- ⁴⁰A. L. Fetter and J. D. Walecka, *Quantum Theory of Many-Particle Systems* (McGraw-Hill, New York, 1971).
- ⁴¹E. Engel and A. Facco Bonetti, *Int. J. Mod. Phys. B* **15**, 1703 (2001).
- ⁴²D. C. Langreth and J. P. Perdew, *Phys. Rev. B* **15**, 2884 (1977).
- ⁴³M. Hellgren and U. von Barth, *Phys. Rev. B* **76**, 075107 (2007).
- ⁴⁴C. D. Hu and D. C. Langreth, *Phys. Rev. B* **33**, 943 (1986).
- ⁴⁵R. W. Godby, M. Schlüter, and L. J. Sham, *Phys. Rev. B* **36**, 6497 (1987).
- ⁴⁶T. Kotani, *J. Phys.: Condens. Matter* **10**, 9241 (1998).
- ⁴⁷A. Facco Bonetti, E. Engel, R. N. Schmid, and R. M. Dreizler, *Phys. Rev. Lett.* **90**, 219302 (2003).
- ⁴⁸Y. M. Niquet, M. Fuchs, and X. Gonze, *J. Chem. Phys.* **118**, 9504 (2003).
- ⁴⁹Y. M. Niquet, M. Fuchs, and X. Gonze, *Phys. Rev. A* **68**, 032507 (2003).
- ⁵⁰M. Grüning, A. Marini, and A. Rubio, *J. Chem. Phys.* **124**, 154108 (2006).
- ⁵¹L. J. Sham and M. Schlüter, *Phys. Rev. Lett.* **51**, 1888 (1983).
- ⁵²D. C. Langreth and J. P. Perdew, *Solid State Commun.* **17**, 1425 (1975).
- ⁵³E. K. U. Gross and W. Kohn, *Phys. Rev. Lett.* **55**, 2850 (1985).
- ⁵⁴E. K. U. Gross, J. F. Dobson, and M. Petersilka, in *Density Functional Theory II*, Topics in Current Chemistry Vol. 181, edited by R. F. Nalewajski (Springer, Berlin, 1996), p. 81.
- ⁵⁵G. Onida, L. Reining, and A. Rubio, *Rev. Mod. Phys.* **74**, 601 (2002).
- ⁵⁶E. Engel and H. Jiang, *Int. J. Quantum Chem.* **106**, 3242 (2006).
- ⁵⁷H. P. Kelly, *Phys. Rev.* **136**, B896 (1964).
- ⁵⁸E. Engel, H. Jiang, and A. Facco Bonetti, *Phys. Rev. A* **72**, 052503 (2005).
- ⁵⁹W. Yang and Q. Wu, *Phys. Rev. Lett.* **89**, 143002 (2002).
- ⁶⁰C. J. Umrigar and X. Gonze, *Phys. Rev. A* **50**, 3827 (1994).
- ⁶¹M. van Faassen and K. Burke, *J. Chem. Phys.* **124**, 094102 (2006).
- ⁶²S. J. Chakravorty, S. R. Gwaltney, E. R. Davidson, F. A. Parpia, and C. Froese Fischer, *Phys. Rev. A* **47**, 3649 (1993).